# Thermoelectric-based cooling system for high-speed motorized spindle II: Optimization and validation strategy

**Fan Kai-Guo** ( fkg11@163.com )
University of Shanghai for Science and Technology
**Rongfei Xu**
University of Shanghai for Science and Technology
**Ruoda Wang**
University of Shanghai for Science and Technology
**Rui Gao**
University of Shanghai for Science and Technology

**Research Article**

**Keywords:** Optimization strategy, Heat transfer path, Simulation and experiment, Cooling system, High-speed motorized spindle

**Posted Date:** September 16th, 2021

**DOI:** https://doi.org/10.21203/rs.3.rs-895120/v1

# Thermoelectric-based cooling system for high-speed motorized spindle Ⅱ: Optimization and validation strategy

Kaiguo Fan*, Rongfei Xu, Ruoda Wang, Rui Gao

School of Mechanical Engineering, University of Shanghai for Science and Technology, Shanghai 200093, China

Corresponding author. E-mail address: fkg11@163.com (K.G. Fan).

**Abstract**

With the development of motorized spindle, the cooling effect and the distribution of cooling capacity become the crucial problem of cooling system. An optimization method for ThermoElectric-based Cooling System (TECS) is proposed based on the conservation of energy to distribute the cooling capacity. The main strategy of the proposed optimization method is to make the cold and heat input at different regions of the spindle sleeve equal in real-time through optimizing the contact area between the Heat Conduction Sleeve (HCS) and spindle sleeve. The numerical simulation and thermal characteristics experiments are carried to verify the effect of the proposed optimization method and the TECS. The simulation and experimental results show that the maximum temperature rise and thermal elongation of the TECS-based motorized spindle are reduced 56.7% and 58.6% compared with water-cooled motorized spindle, and the temperature distribution of the spindle sleeve is more uniform. It is meaningful to improve the accuracy of motorized spindle.

**Keywords**

Optimization strategy, Heat transfer path, Simulation and experiment, Cooling system, High-speed motorized spindle

## 1. Introduction

The heats generated by the internal heat sources transfer to the environment and the cooling system through different components and contact surfaces, which forms a heat transfer path. The purpose of thermal optimization is to optimize the heat transfer path to reduce the temperature rise and thermal deformation. The internal heat sources, thermal conductivity, thermal contact resistance, convective heat transfer, and the structure of these components are the main factors that affect the heat transfer path.

In order to optimize the heat transfer path, the first step is to obtain the thermal behavior of a machine tool which is usually realized through numerical simulation. Before simulation, the thermal boundary conditions, which include the heat generation of internal heat sources, the thermal contact resistance, and the convection coefficient, should be determined firstly. The internal heat sources of a machine tool mainly include the heat converted from the motor energy consumption which can be calculated through the measured motor torque [1, 2] and empirical formulas etc., the heat generated by friction of rotation and transmission components which can be determined through calculating the friction torque using the empirical formula [3, 4] etc., and the heat generated by cutting which can be calculated through reverse solving of differential equation of unsteady heat conduction according to the actually measured temperature of the cutting tool [5]. The commonly used identification methods of thermal contact resistance mainly include the theoretical calculation method [6-8] and the experimental method [9-11] to obtain the thermal contact resistance under a specific working condition. For the calculation of convection coefficient, Chow etc. [12] proposed a prediction model using the method of finite difference and experiment. Barrios etc. [13] used the finite volume method and Gaussian method to establish a three-dimensional transient model for convection coefficient which can realize the calculation of convection coefficient under cutting conditions.

After determining the thermal boundary conditions, the finite element numerical simulation is usually used to analyze the thermal behavior of the machine tool. References [14, 15] used the finite element numerical simulation method to analyze the temperature field and thermal deformation of machine tool's spindle and ball screw, which can reveal the heat transfer path of a machine tool and can guide the optimization design of the machine tool. However, the simulation accuracy depends on the calculation accuracy of boundary conditions. There are many parameters should be calculated accurately to obtain the most realistic boundary conditions and simulation results. Some parameters, such as the spindle speed, rated power, surface roughness, hardness, thermal conductivity, elastic modulus, Poisson's ratio, and the dimension of part can be identified accurately according to the material properties and the machine tool's parameters. However, some parameters, such as the friction torque of bearing and contact pressure between the contact surfaces are very difficult to calculate accurately due to the influence of manufacturing and assembly accuracy of machine tool's parts. Furthermore, the friction torque of bearing and contact pressure between contact surfaces will change with thermal deformation of machine tool's components. In order to improve the calculation accuracy of thermal boundary conditions, Kang etc. [16] established a dynamic heat generation model for bearing considering the thermally-induced preload and the viscosity-temperature effects, which greatly improves the calculation accuracy of heat generation of bearing. Fan [17] used the temperature rise of thermal key points to real-timely correct the heat generation of internal heat

sources which can effectively improve the simulation accuracy. However, since the thermal boundary conditions of a machine tool are very complicated, it is difficult to obtain its actual value.

Using the simulation results, the heat transfer path of the machine tool can be optimized. For the structural optimization, the main methods include the construction theory, topology optimization, and bionic optimization to optimize the material distribution within a specific load, constraint, area, and performance [18-20]. For the optimization of convective heat transfer, the commonly used method is to increase the heat dissipation of the cooling system and balance the temperature field through controlling the cooling parameters and optimizing the cooling channel [21-24]. For the optimization of thermal conductivity, the material with high thermal conductivity becomes the best choice, through which the heats generated by the internal heat sources can be transferred to other areas quickly to balance the temperature field [25]. The thermal contact resistance between the contact surfaces is affected by factors such as the intermediate medium, material properties, roughness of contact surfaces, temperature, and pressure etc. [26-29], the current research mainly focuses on the analysis of above factors and attempts to optimize these factors. In summary, the above studies provide a basis for the optimization of heat transfer path.

After optimization, the numerical simulation and thermal characteristics experiment are usually used to verify the optimization effect. The advantage of numerical simulation is that it can solve complex nonlinear problems and simulate the thermal characteristics of whole machine. But the simulation accuracy depends on the calculation accuracy of thermal boundary conditions, finite element model, etc. In order to obtain the more realistic thermal behavior of a machine tool, the thermal characteristics experiment has been the best choice. The thermal characteristics experiment of a machine tool includes the spindle idling experiment under different spindle speed and running time, the environmental temperature variation error (ETVE) test, the test for thermal distortion caused by moving linear axes, the test for thermal distortion caused by rotary motion of components [30], etc. The commonly used test devices include the temperature and displacement sensors to measure the temperatures of thermal key points and the thermal deformation of key components of the machine tool. With the development of detection technology, thermal imaging and laser techniques have been applied to the temperature and displacement sensors to achieve non-contact measurement. Wu etc. [31] used the thermal infrared imager and laser triangulation sensors to measure the temperature field and thermal deformation of a motorized spindle, the significant effect of the high rotational speeds, preload oil viscosity, and heat transfer coefficients on the temperature or thermal failure of the bearing has been revealed. However, the thermal characteristics test method is limited by the number of measuring sensors and the installation location, and cannot fully reflect the thermal behavior especially the internal thermal behavior of a machine tool.

In summary, the thermal behavior of a machine tool is like a "black box", there are many factors that can only be obtained through experience and theory, which limits the accuracy of thermal optimization and thermal behavior analysis. In order to solve this problem, an online correction method for thermal boundary conditions is proposed in Part 1 which can improve the simulation accuracy significantly. In this study, the corrected thermal boundary conditions are used to simulate the thermal behavior of a motorized spindle and the simulation results is used to optimize the heat transfer path. The optimization strategy is introduced in section 2. The optimization effect of the ThermoElectric-based Cooling System (TECS) is verified through numerical simulation and thermal characteristics experiment in section 3 and 4. Finally, some discussions about the cooling effect and cooling system are given in section 5.

## 2. Optimization strategy of TECS

The optimization strategy of the TECS is to make the cold and heat input at different regions of the spindle sleeve equal in real-time through optimizing the contact area between the Heat Conduction Sleeve (HCS) and spindle sleeve as shown in **Fig. 1**. The detailed optimization strategy is as follows,

1) Extracting the temperature rise of the spindle sleeve along the axial direction as shown in **Fig. 2**.
2) Fitting the temperature rise of the spindle sleeve as a linear function of axial position.
3) Modifying the linear function established in previous step using the following equations,

$$c_{SP} \cdot \rho_{SP} \cdot 2\pi rt(\Delta l \sum_{i=1}^{n} \Delta T_i - \int_0^l f(x)dx) = 0 \tag{1}$$

$$f(x) = p_1 x + p_2 \tag{2}$$

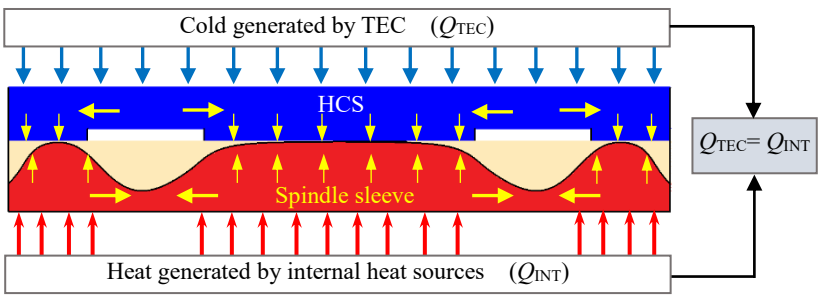


**Fig. 1.** The optimization mechanism of the TECS shows that the cooling capacity generated by the TEC is distributed through optimizing the contact area between the HCS and spindle sleeve.

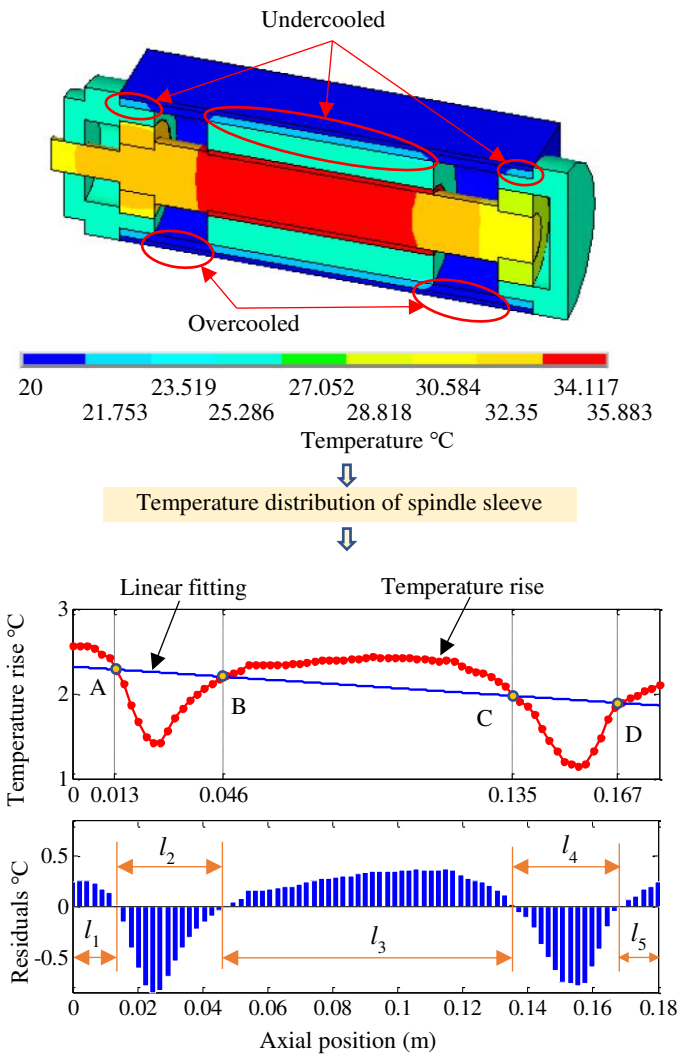


**Fig. 2.** The temperature distribution of spindle sleeve is used to optimize the HCS through linear fitting of temperature rise.

where, $c_{SP}$ and $\rho_{SP}$ are the specific heating capacity in J/(kg·℃) and density in kg/m$^3$ of the spindle sleeve, respectively, $r$ and $t$ are the average radius and wall thickness of the spindle sleeve in meter, respectively, $x$ is the axial position of the spindle sleeve in meter, $\Delta l$ and $\Delta T_i$ are the length in meter and temperature rise of each section of the spindle sleeve, respectively, $n$ is the number of the extracted temperature rises.

Substituting Eq. (2) into Eq. (1), the following equation can be obtained,

$$\Delta l\sum_{i=1}^{n}\Delta T_i-\frac{1}{2}p_1l^2-p_2l=0 \tag{3}$$

where, $l$ is the length of the spindle sleeve in meter, $p_2$ is the coefficient to be revised. In Eq. (3), $\Delta l$, $\Delta T_i$, and $l$ are all known, $p_1$ can be obtained through the linear fitting of temperature rise established in step 2). In order to make Eq. (1) true, we only need to calculate the coefficient of $p_2$ through Eq. (3). Then, a new linear function of temperature rise can be established as shown in Fig. 2.

4) Calculating the intersections of the temperature rise curve and the new fitting line, and marking the intersections as A, B, C, and D as shown in Fig. 2.
5) Calculating the lengths of $l_1$ through $l_5$ according to the calculated intersections of A, B, C, and D.

Using the above-mentioned method, the length of each section of the spindle sleeve can be calculated as $l_1$=0.013 m, $l_2$=0.033 m, $l_3$=0.089 m, $l_4$=0.032 m, and $l_5$=0.013 m. It can be seen from Fig. 2 that the temperature rises at regions $l_1$, $l_3$, and $l_5$ are higher than that at regions $l_2$ and $l_4$. On the one hand, because the heats at regions $l_2$ and $l_4$ are transferred from regions $l_1$, $l_3$, and $l_5$ and then transferred to the HCS, reducing the heat transfer from regions $l_2$ and $l_4$ to the HCS can increase the temperature rise at regions $l_2$ and $l_4$. On the other hand, because the cooling capacity generated by the TEC are constant at a certain moment, reducing the input of cooling capacity at regions $l_2$ and $l_4$ can increase the input of cooling capacity at regions $l_1$, $l_3$, and $l_5$. Therefore, reducing the contact area between the HCS and spindle sleeve at regions $l_2$ and $l_4$ can increase the temperature rise at regions $l_2$ and $l_4$ and decrease the temperature rise at regions $l_1$, $l_3$, and $l_5$. The removed widths are equal to $l_2$ and $l_4$ as shown in Fig. 3. Thereby, the structure of the HCS is optimized through the above-mentioned optimization method.

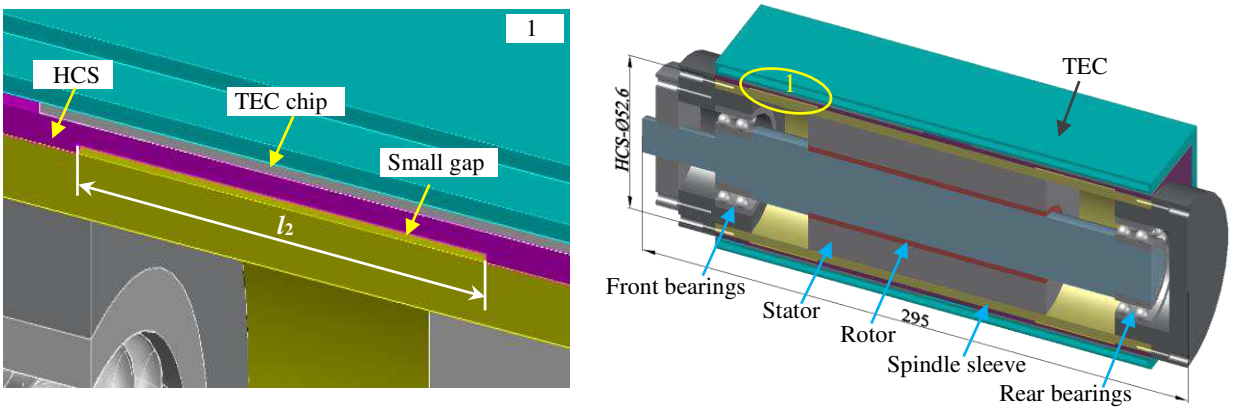


**Fig. 3.** The motorized spindle is re-equipped using the TECS to replace the water-cooling system.

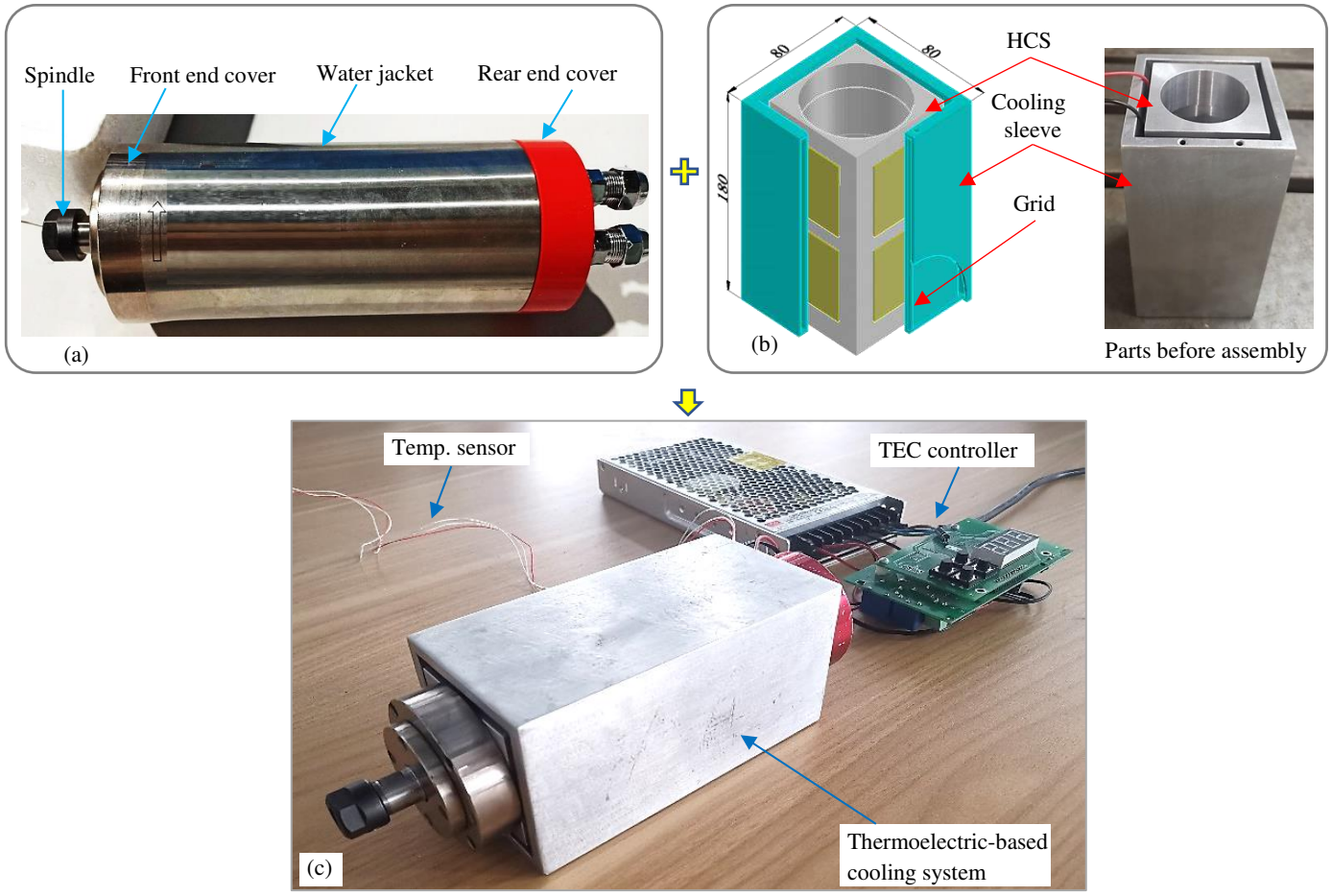


(a) Water-cold motorized spindle (b) TECS (c) TECS-based motorized spindle

**Fig. 4.** The structure of the motorized spindle before and after re-equipped shows that the water jacket of the water-cooled motorized spindle is replaced by the TECS.

In summary, the design and optimization strategy of the proposed TECS includes 5 steps. The first step is calculating the parameters of HCS to achieve the purpose of rapid heat conduction using the constrained optimization method. The second step is determining the required maximum cooling power and number of thermoelectric cooling chips used in ThermoElectric Cooler (TEC) to cool the heat transferred to the HCS completely according to the maximum heats generated by the internal heat sources and the structure of the motorized spindle. The third step is designing the cooling sleeve to cool the hot side of the TEC according to the maximum heat generation of the motorized spindle and the power consumption of the TEC. The fourth step is designing the TEC controller to control the cooling capacity of the TEC based on the Proportion Integral Differential (PID) algorithm. The fifth step is optimizing the structure of HCS to distribute the cooling capacity accurately according the temperature distribution of the spindle sleeve.

Using the above-mentioned 5 steps to design and optimize the TEC and HCS, a TECS-based motorized spindle can be designed or re-equipped. **Figure 4** shows the structure of the motorized spindle before and after re-equipped. In order to compare the cooling effect of TECS with water-cooling system, the numerical simulation of the motorized spindle before and after re-equipped are carried out in section 3.

## 3. Simulation validation

### *3.1 Thermal behavior simulation*

The simulation conditions are that the spindle speed is 6000 rpm, the temperatures of ambient and cooling water are all 20 ℃, the temperature of the cold side of TEC is set as 20 ℃, that is the temperature of HCS is 20 ℃ due to the cold side of TEC is HCS. The structures of the stator and bearings are simplified as cylinders, some small structures in the finite element model, such as bolts, bolt holes, chamfers, etc., are removed. All the corrected boundary conditions (as shown in **Table 1**) and structures of the motorized spindle before and after re-equipped are the same except for the cooling system in numerical simulations. Applying the corrected boundary conditions to the finite element model, the temperature field of the motorized spindle before and after re-equipped can be obtained as shown in **Fig. 5**.

**Table 1**
Calculation of initial boundary conditions and its corrected results.

| Boundary conditions | Assemblies/Medium | Initial conditions | Calculation equations | Calculated results | Corrected results |
|---|---|---|---|---|---|
| Heat generation | Front bearings<br>Rear bearings | $n$=6000 rpm | $Q_b = 1.047\times10^{-4} nM$ | 8.5 W<br>6.8 W | 8.3 W<br>6.5 W |
| | Stator<br>Rotor | $P_r$=0.8 kW<br>$P$=6%<br>$\eta$=0<br>$Q_s$=2×$Q_m$/3<br>$Q_r$=$Q_m$/3 | $Q_m = (1-\eta)PP_r$ | 32 W<br>16 W | 30.8 W<br>15.4 W |
| Thermal contact resistance | Spindle to bearing<br>Bearing to bearing sleeve<br>Bearing sleeve to spindle sleeve<br>Spindle sleeve to HCS<br>Stator to housing | $\sigma_1$=0.8 μm<br>$\sigma_2$=0.8 μm<br>$\varepsilon$=0.02~0.06 mm | $R_c = \frac{\sigma}{105.6\times k}\times(\frac{H}{P})^{0.618}$ | 8.6×10$^{-4}$ m$^2$·K/W<br>9.5×10$^{-4}$ m$^2$·K/W<br>9.8×10$^{-4}$ m$^2$·K/W<br>5.1×10$^{-4}$ m$^2$·K/W<br>9.8×10$^{-4}$ m$^2$·K/W | 9.8×10$^{-4}$ m$^2$·K/W<br>10.1×10$^{-4}$ m$^2$·K/W<br>10.5×10$^{-4}$ m$^2$·K/W<br>8.1×10$^{-4}$ m$^2$·K/W<br>10.5×10$^{-4}$ m$^2$·K/W |
| | Rotor to stator | | Compound heat transfer | 1×10$^{-2}$ m$^2$·K/W | 1×10$^{-2}$ m$^2$·K/W |
| Convection coefficient | Water<br>Air | $v_{water}$=0.3 m/s | $h = \frac{Nu\cdot k_{fluid}}{L}$ | 251.6 W/(m$^2$·K)<br>9.7 W/(m$^2$·K) | 235.8 W/(m$^2$·K)<br>8.9 W/(m$^2$·K) |
| Temperature | TEC<br>Water<br>Ambient | 20 ℃ | Preset | 20 ℃<br>20 ℃<br>20 ℃ | 20 ℃<br>20 ℃<br>20 ℃ |

**Figure 5 (a)** shows the temperature field of the motorized spindle with water-cooling system. The maximum temperature rise of the motorized spindle is 32.302 ℃ which occurs in the rotor. The temperature distribution of the spindle sleeve is ununiform, the temperature rises at the regions related to the internal heat sources are higher than that at other regions, and the maximum temperature difference of the spindle sleeve is 3.105 ℃. The minimum temperature rise is 5.513 ℃ which occurs in the cooling water jacket. That is, the water-cooling system cannot dissipate the heat transferred to the cooling channel completely when the water temperature is the room temperature.

**Figure 5 (b)** shows the temperature field of the motorized spindle with TECS. The maximum temperature rise of the motorized spindle is 15.611 ℃ which occurs in the rotor. The temperature distribution of the spindle sleeve is more uniform, and the maximum temperature difference is 0.547 ℃. The minimum temperature rise is 0 ℃ which occurs in the HCS. That is, the TECS can cold the heat transferred to the HCS completely.

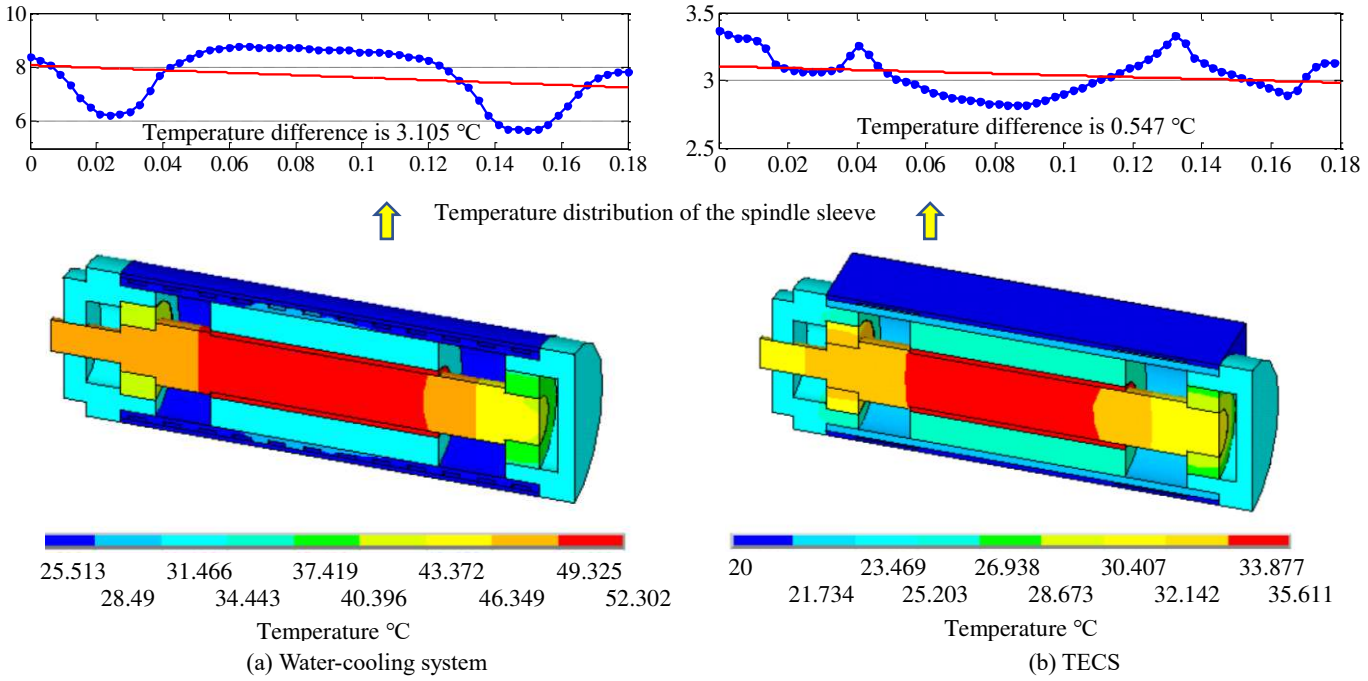


**Fig. 5.** Simulation result shows the temperature field of the motorized spindle before and after re-equipped. The temperature field of the spindle sleeve with TECS is more uniform than that with water-cooling system.

Comparing **Fig.5 (a)** with **(b)**, the temperature distribution of the spindle sleeve with TECS is more uniform than that with water-cooling system, the maximum temperature difference of the spindle sleeve is reduced from 3.105 ℃ to 0.547 ℃. That is, the optimization design of HCS can distribute the cooling capacity effectively. The maximum temperature rises of the TECS-based motorized spindle is reduced 16.691 ℃ compared with water-cooling system. That is, the cooling effect of the TECS is significantly better than that of water-cooling system when the water temperature is the room temperature. The simulation results also show that the temperature distribution of the motorized spindle before and after re-equipped is basically the same except for the spindle sleeve and cooling system. That is, changing the structure of the motorized spindle can improve the temperature field distribution, which can be used to guide the thermal optimization design of the motorized spindle.

### *3.2 Stiffness simulation*

Because the water-cooling system is replaced by the TECS, and the structure of the two is different, the modal analysis is carried out to verify the stiffness of the motorized spindle before and after re-equipped. The simulation conditions are that the front end of the motorized spindle is fixed while the rear end only restricts the radial displacement, all contact surfaces are bounded, the density, elastic modulus, and Poisson's ratio of steel and AL 6063 are 7800 and 2700 kg/m$^3$, 211 and 69 Gpa, 0.3 and 0.33, respectively, a force of 100 N is applied to the front end of the spindle. The number of modes to be extracted is set as 6.

**Figure 6** shows the first-, third-, and fifth-orders vibration modes, **Table 2** shows the first six orders frequencies of the motorized spindle before and after re-equipped. The simulation results show that the stiffness of TECS-based motorized spindle has little change compared with water-cooled motorized spindle, the vibration modes before and after re-equipped are almost the same, the first- and sixth-orders frequencies are slightly lower than water-cooled motorized spindle, but the other orders frequencies are higher than water-cooled motorized spindle. In theory, the first-order frequency of the TECS-based motorized spindle decreases, the other orders frequencies also should decrease. However, the simulation results are inconsistent with the theory, the first- and sixth-orders frequencies decrease but the other orders frequencies increase. This is because the main structure of the motorized spindle before and after re-equipped is the same except for the cooling system, and the constraint position and mode are the same too, the stiffness of the motorized spindle changes little before and after re-equipped.

On the other hand, the finite element method is based on the discretization which will lead to deviations from the actual continuum. In addition, the boundary conditions of the actual continuum are very complicated, and the finite element method cannot fully simulate these boundaries. Therefore, there is a certain deviation between the simulated and actual values. In order to verify the stiffness of the motorized spindle before and after re-equipped, the vibration test under cutting conditions is carried out in section 4.2.

**Table 2**
Simulated natural frequencies of the motorized spindle before and after re-equipped.

| | Water-cooled motorized spindle (Hz) | TECS-based motorized spindle (Hz) |
|---|---|---|
| 1st order | 604.87 | 591.53 |
| 2nd order | 1688.0 | 1774.7 |
| 3rd order | 1961.5 | 2259.1 |
| 4th order | 2134.6 | 2639.6 |
| 5th order | 2913.0 | 2962.7 |
| 6th order | 3429.2 | 3352.0 |

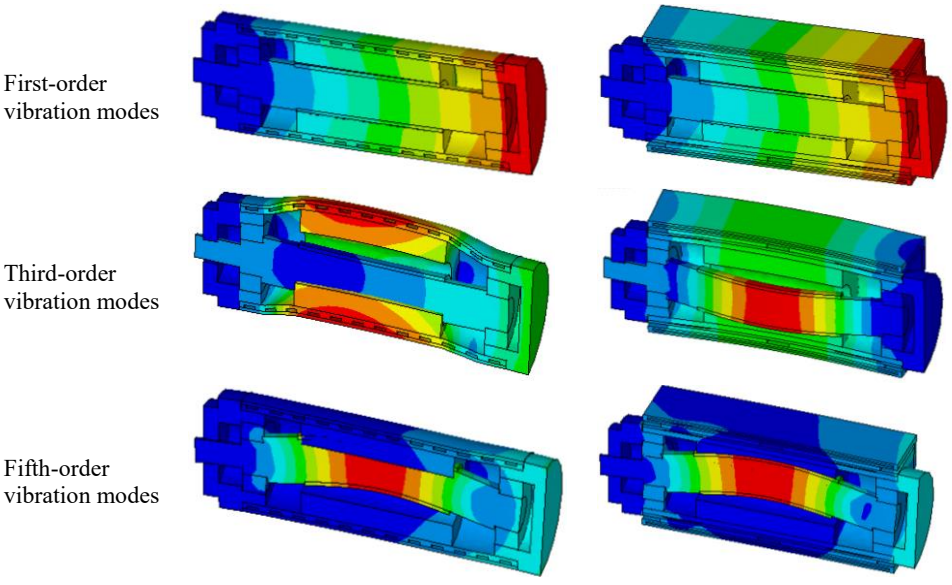


(a) Water-cooled motorized spindle (b) TECS-based motorized spindle

**Fig. 6.** Simulated vibration modes of the motorized spindle before and after re-equipped.

## 4. Experimental validation

### *4.1 Thermal behavior validation*

In order to verify and compare the actual effect of the TECS-based motorized spindle with water-cooled motorized spindle, the thermal characteristics experiments of the motorized spindle before and after re-equipped are carried out respectively, the temperature rise of the front bearing cap and the thermal elongation of the spindle are used to characterize the thermal characteristics of the motorized spindle.

**Figure 7 (a)** shows the experimental setup of water-cooled motorized spindle. The motorized spindle is fixed in a vise, the frequency converter is used to control the spindle speed. An eddy current displacement sensor is used to measure the thermal elongation of the spindle. The temperature sensors T1, T2, and T3 are used to measure the temperature rise of the spindle related to the internal heat sources which is the front bearings, stator, and rear bearings, respectively. The experiment is divided into three groups according to the spindle speed which is 3000, 6000, and 10000 rpm, respectively. A pump is used to circulate the cooling water in the coolant channel, the temperature of the cooling water is 22 ℃, and the flow rate is 0.3 m/s. Each experiment starts from the cold state, and the ambient temperature of the laboratory is 22 ℃.

**Figure 7 (b)** shows the measured and simulated temperature rises of the spindle housing at the measurement position T1 when the spindle speed is 3000, 6000, 10000 rpm, respectively. It can be seen from **Fig. 7 (b)** that the thermal equilibrium time of the spindle housing is about 1500 seconds, and the temperature rise trends of the front bearing cap under different spindle speed are the same. The maximum temperature rise of the front bearing cap is 13.2 ℃ which occurs when the spindle speed is 10000 rpm. **Figure 7 (b)** also shows that the simulation results are consistent with the experimental results, and the simulation accuracy is great than 95% using the online correction method to correct the thermal boundary conditions. This proves that the proposed online correction strategy for thermal boundary conditions can effectively improve the simulation accuracy of thermal characteristics of machine tool.

**Figure. 8 (a)** shows the thermal elongation of the spindle, the maximum thermal elongation of the spindle is 44.85 μm when the spindle speed is 10000 rpm. The thermal elongation trend of the spindle is consistent with the temperature rise trend of the front bearing cap. **Table 3** shows the maximum thermal elongation of the spindle before and after re-equipped when the spindle speed is 3000, 6000, and 10000 rpm, respectively.

**Figure 9 (a)** shows the experimental setup of the TECS-based motorized spindle. The water-cooling system is replaced by the TECS. The motorized spindle is fixed in a vise. The TEC controller designed in Part 1 is used to control the temperature of the HCS, and the preset temperature of the HCS is ambient temperature. The temperature and displacement sensors used in this experiment are the same with the experiment of water-cooled motorized spindle, but the measurement positions of the temperature sensors are different. The temperature sensors T1 and T2 are used to measure the temperature rises of front and rear bearing caps, the temperature sensor T3 is used to measure the temperature rise of the HCS in this experiment. Temperature sensor $T_{HCS}$ is used to control the cooling power through the TEC controller. The experiment is divided into three groups according to the spindle speed which is 3000, 6000, and 10000 rpm, respectively.

**Table 3**
Thermal elongation of the spindle before and after re-equipped.

| Cooling mode | Thermal elongation of the spindle (μm) | | |
|---|---|---|---|
| | 3000 rpm | 6000 rpm | 10000 rpm |
| Water-cooling | 13.59 | 32.62 | 44.85 |
| TEC | 6.13 | 13.98 | 18.57 |

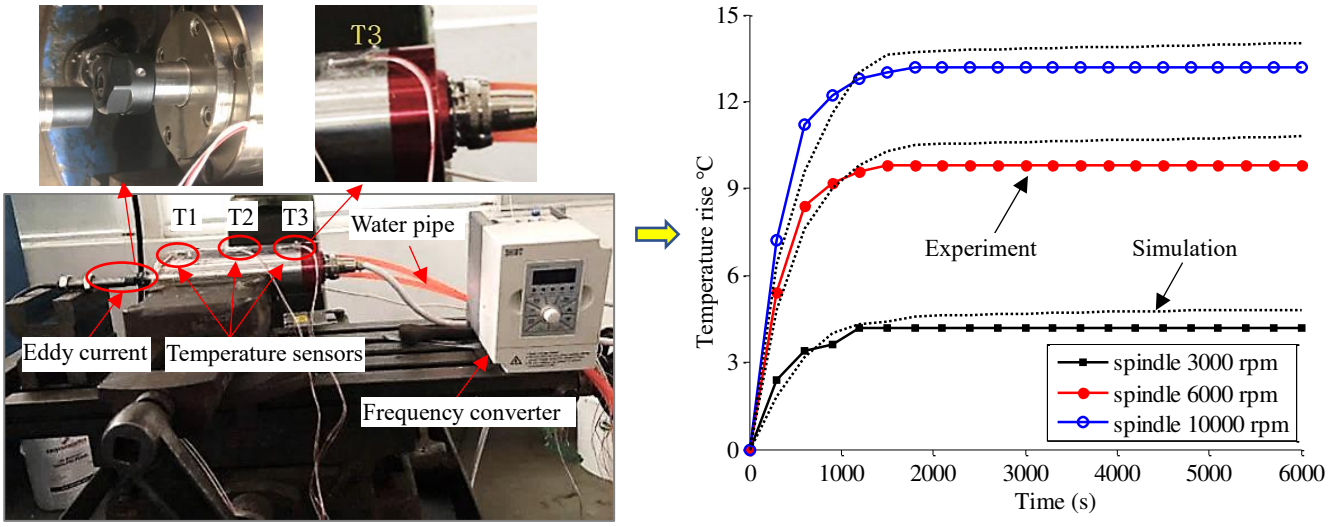


(a) Experimental setup

(b) Temperature rise of the front bearing cap

**Fig. 7.** Actual experimental setup shows a water-cooled motorized spindle clamped in a vise. Three temperature sensors and an eddy current are used to measure the temperature and thermal elongation of the spindle.

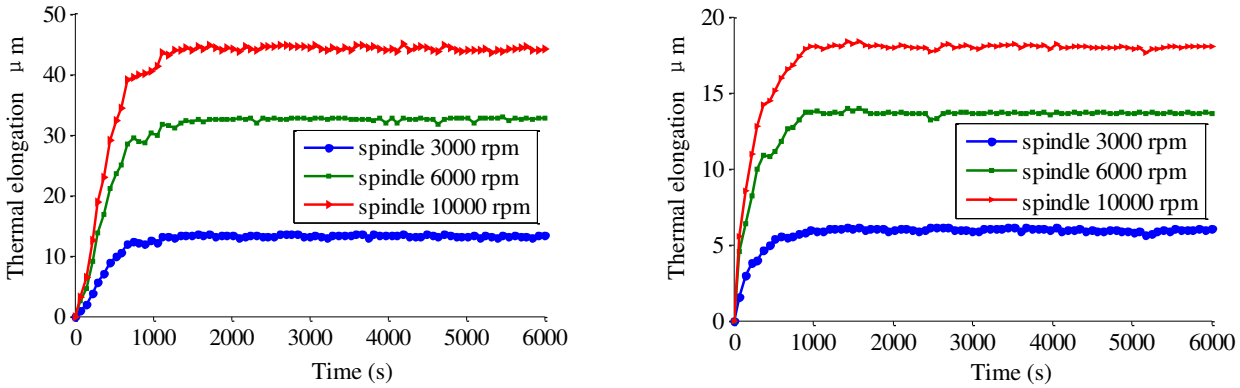


**Fig. 8.** Experimental result shows the thermal elongation of the motorized spindle before and after re-equipped. The thermal elongation of the TECS-based motorized spindle is significantly improved.

**Figure 9 (b)** shows the temperature rises measured by the temperature sensor T1 when the spindle speed is 3000, 6000, 10000 rpm, respectively. The maximum temperature rise of the front bearing cap is 5.7 ℃ which is reduced 56.7% compared with water-cooled motorized spindle. **Fig. 9 (b)** also shows that the simulation results are consistent with the experimental results, and the simulation accuracy is great than 95% using the online correction method to correct the thermal boundary conditions. The maximum thermal elongation is 18.57 μm when the spindle speed is 10000 rpm as shown in **Fig. 8 (b)**, which is reduced 58.6% compared with water-cooled motorized spindle.

Comparing the thermal characteristics of TECS-based motorized spindle with water-cooled motorized spindle as shown in **Figs. (7, b)**, **(8)**, and **(9, b)**, the trends of temperature rise and thermal elongation of the motorized spindle before and after re-equipped are almost the same, this is because the main structure of the motorized spindle is the same, and the heat transfer in the motorized spindle is the same too except for the cooling system. But the temperature rises and thermal elongation of the TECS-based motorized spindle is significantly reduced compared with water-cooled motorized spindle, which proves that the cooling effect of the TECS is significantly better than that of water-cooling system. It is meaningful to improve the accuracy of motorized spindle.

In order to further verify the control effect of the TECS, another two experiments are carried out in this study. The first experiment is to verify the control effect of the TECS under different conditions, the ISO 230-3 standard is used to test the thermal elongation of spindle and the temperature of HCS as shown in **Fig. 10**. The experimental result shows that the temperature of the HCS is controlled within 0.2 ℃, which verifies the control effect of the TECS. The thermal elongation of the spindle increases continually, but the increasing trend is different from that of single spindle speed due to the change of spindle speed during its running.

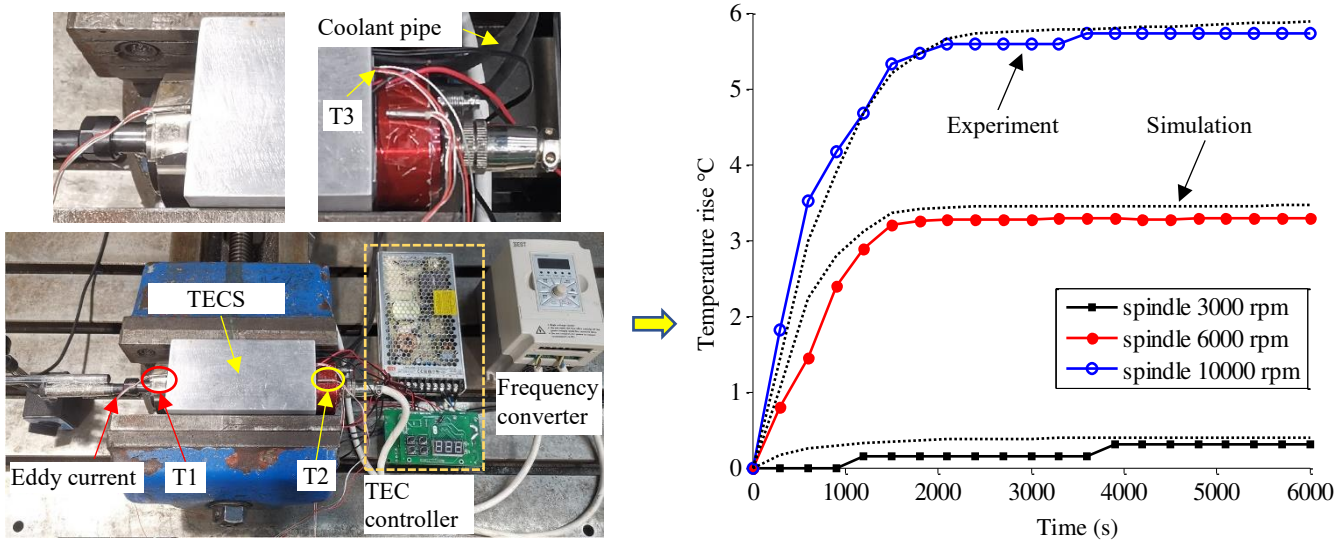


**Fig. 9.** Actual experimental setup shows the TECS-based motorized spindle clamped in a vise. Three temperature sensors and an eddy current are used to measure the temperature and thermal elongation of the spindle to compare the cooling effect with water-cooling system.

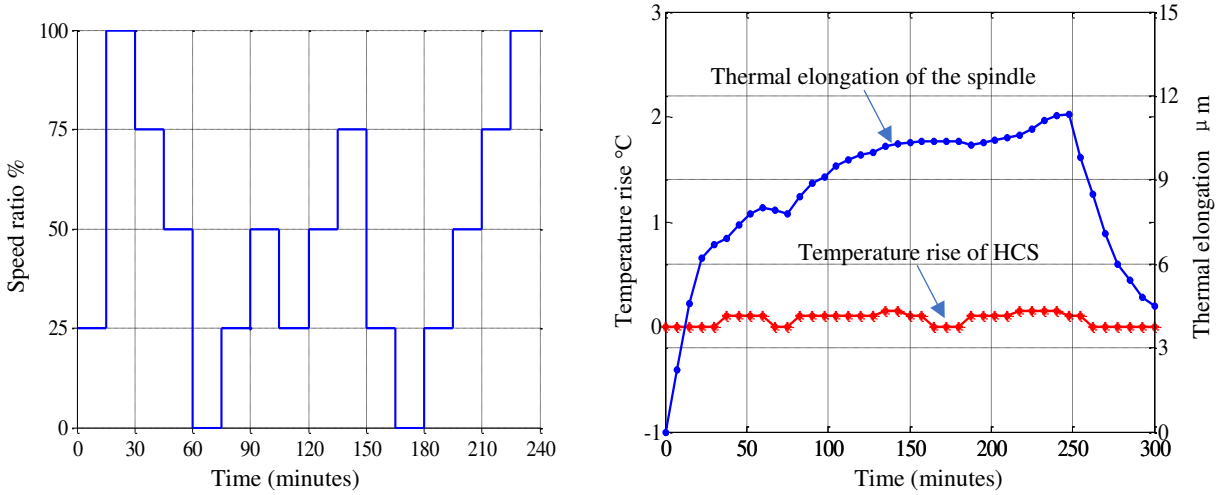


**Fig. 10.** Control effect validation of TECS using the ISO 230-3 standard.

The second experiment is to verify the influence of the control temperature of HCS on the thermal elongation of the spindle. The control temperature of the HCS is set to 5, 10, 15, 20 °C lower than the ambient temperature, respectively, and the spindle speed is 6000 rpm. The experimental results show that the thermal elongation of the spindle decreases with the decrease of the control temperature of HCS as shown in **Fig. 11**. When the temperature of the HCS is 15 °C lower than the ambient temperature, the thermal deformation of the spindle is close to zero. That is to say, control the temperature of HCS can cool the motorized spindle deeply, which is of significance to improve the accuracy of motorized spindle. However, when the controlled temperature of the HCS is much lower than the ambient temperature, the condensed water will be generated on the surface of motorized spindle, the appropriate temperature without condensed water generated needs further study.

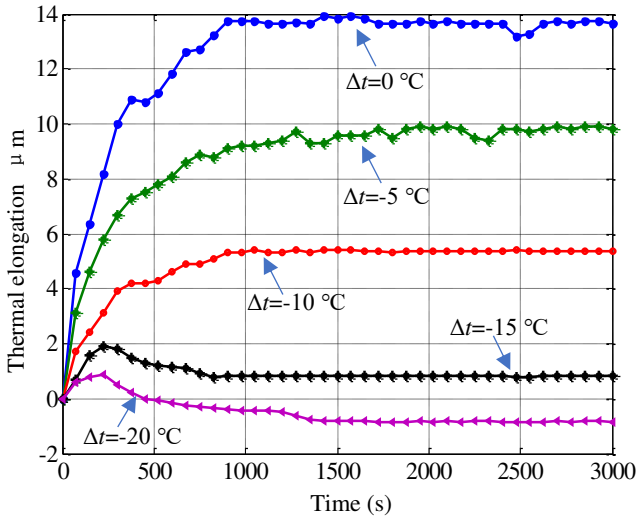


**Fig. 11.** The thermal elongation of the spindle decreases with the decrease of the control temperature of HCS. Δ*t* is the temperature difference between the HCS and ambient.

According to the experimental results, the cooling effect of the proposed TECS is obviously better than that of water-cooling system, and the proposed TECS can realize the deep cooling of motorized spindle to achieve the goal of zero thermal elongation of motorized spindle, which is of great significance to improve the performance and machining accuracy of motorized spindle.

### *4.2 Stiffness validation*

In order to verify the influence of TECS on the stiffness of the motorized spindle, a vibration test is carried out under the cutting condition. **Figure 12** shows the experimental setup of the stiffness validation of the motorized spindle before and after re-equipped. The motorized spindle is fixed on a small-sized CNC machine tool through a flange used to fix the front end and a fixture used to restrict the radial displacement of the rear end. Because acceleration is generally used for vibration evaluation of high-speed rotating machinery, an acceleration sensor is installed on the rear end of the motorized spindle to measure its vibration acceleration in this experiment. The experimental conditions are that the spindle speed is 6000 rpm, the feed rate of the cutting tool is 0.2 mm/r, the workpiece material is aluminum alloy. The measured maximum vibration accelerations of the water-cooled motorized spindle and the TECS-based motorized spindle are 3.89 g and 3.91 g, respectively. The experimental results show that the stiffness of TECS-based motorized spindle has little change compared with water-cooled motorized spindle, which is consistent with the simulation results as shown in section 3.2.

## 5. Discussions

### *5.1. Discussion about the cooling effect*

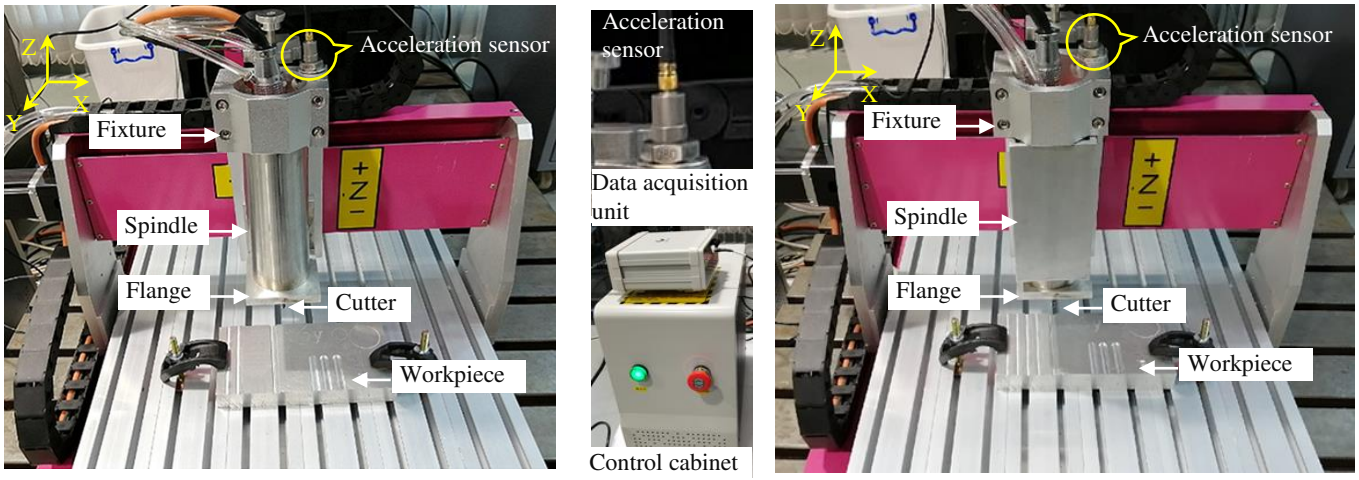


(a) Water-cooling system

(b) TECS

**Fig. 12.** Actual experimental setup shows the motorized spindle installed in a small-sized CNC machine tool to verify the stiffness. An acceleration sensor is used to measure the vibration acceleration of the spindle.

According to the experiment results, the temperature of the cold side of the TEC can be controlled by controlling the electric current passing through the TEC as shown in section 4.1. That is, the temperature of HCS can be controlled real-timely due to the cold side of TEC is HCS. However, it is difficult to control the temperature of cooling channel in water-cooled motorized spindle. According to the heat transfer theory, the heat transferred to the HCS of the TECS-based motorized spindle and the cooling channel of water-cooled motorized spindle at the steady state can be calculated by Eqs. **(4)** and **(5)**, respectively.

$$Q_{hc-T} = \frac{t_{int-T} - t_{HCS}}{\sum R_i} = Q_c \tag{4}$$

$$Q_{hc-w} = \frac{t_{int-w} - t_{channel}}{\sum R_i} = hA(t_{channel} - t_{water}) \tag{5}$$

where, $Q_{hc\text{-}T}$ and $Q_{hc\text{-}w}$ are the heat transferred to the HCS and cooling channel in Watts, respectively, $t_{int\text{-}T}$ and $t_{int\text{-}w}$ are the temperatures of internal heat sources in TECS-based motorized spindle and water-cooled motorized spindle in °C, respectively, $t_{channel}$ and $t_{water}$ are the temperatures of cooling channel and water in °C, respectively, $\sum R_i$ is the total thermal resistance which can be regarded as a constant at the steady state, $h$ is the convection coefficient of cooling water in W/(m$^2$·K), $A$ is the heat exchange area in m$^2$.

Because the heat transferred to the HCS is cooled completely by the TEC real-timely, the temperature of the HCS is equal to the room temperature. Assuming that the heat transferred to the HCS is equal to that transferred to the cooling channel of water-cooled motorized spindle, and the cooling water keeps room temperature, then,

$$t_{\text{int}-T} - t_{HCS} = t_{\text{int}-w} - t_{channel}\ ,\ t_{water} = t_{HCS} = t_a \tag{6}$$

According to the heat transfer theory, the temperature of the cooling channel must be higher than water temperature to achieve the heat transfer in water-cooling system. That is, $t_{channel} > t_{HCS}$, thereby the temperature of the internal heat sources in water-cooled motorized spindle is higher than that in TCES-based motorized spindle, that is $t_{int\text{-}w} > t_{int\text{-}T}$. It means that the cooling effect of TECS is better than that of water-cooling system.

If the heat transferred to the HCS is greater than that transferred to the cooling channel, that is,

$$t_{\text{int}-T} - t_{HCS} > t_{\text{int}-w} - t_{channel}\ ,\ t_{channel} > t_{water} \tag{7}$$

Because the heat generation is consistent under the same condition, there are more heats are converted into the internal energy in water-cooled motorized spindle and its temperature is higher than that in TECS-based motorized spindle. It also means that the cooling effect of TECS is better than that of water-cooling system.

If the heat transferred to the HCS is less than that transferred to the cooling channel, that is,

$$t_{\text{int}-T} - t_{HCS} < t_{\text{int}-w} - t_{channel}\ ,\ t_{channel} > t_{water} \tag{8}$$

Because the temperature of cooling channel is greater than that of HCS, the temperature of the internal heat sources in water-cooled motorized spindle is also higher than that in TCES-based motorized spindle. Therefore, the cooling effect of the TECS is better than water-cooling system when the temperature of the cooling water keeps ambient temperature.

According to the theoretical discussion abovementioned, the cooling effect of the proposed TECS is better than water-cooling system when the cooling water keeps ambient temperature which is consistent with the simulation and experiment results.

### *5.2. Discussion about the cooling system*

Generally, a cooling system of a motorized spindle includes the coolant channel, cooling medium, and drive device for cooling medium. The commonly used coolant channel is rectangular helical channel which is usually installed in the inside of the spindle housing to transfer the heat generated by internal heat sources to the cooling medium. The commonly used cooling medium includes the water, compressed air, and cooling oil, which flows in the coolant channel and dissipates the heat to the environment. The heat dissipation capacity of a cooling system depends on both the coolant channel and the cooling medium.

On the one hand, the structure, material, and interface thermal resistance of coolant channel affect the cooling effect of cooling system. As the heat generation of each internal heat source is different, the temperature field of the cooling sleeve is ununiform. It is difficult to design a suitable coolant channel that does not affect the flow rate and can balance the temperature field. Moreover, the interface thermal resistance will increase with the deposition of dirt. However, the form of HCS is solid, the cooling effect of HCS is not affected by the interface thermal resistance and it is easer to optimize the structure.

On the other hand, the cooling effect of a cooling system is not only related to the structure of coolant channel but also related to the heat absorption capacity and thermal diffusivity of cooling medium, which depends on the thermal conductivity, specific heating capacity, velocity, and flow of cooling medium in traditional cooling system. Due to the influence of the structure of motorized spindle, the velocity and flow of cooling medium are all limited which affect the cooling effect of cooling system. Therefore, accurate modeling and control for heat absorption of traditional cooling system requires in-depth research. However, the thermal diffusivity of HCS depends on the material's properties as shown in Eq. (9).

$$a = \frac{k}{\rho \cdot c} \tag{9}$$

In Eq. (9), $k$, $\rho$, and $c$ are the thermal conductivity, density, and specific heating capacity of the HCS, respectively. Currently, materials with high thermal diffusivity include the diamond, carbon fiber, copper alloys, aluminum alloys, etc. Considering the factors of processability and price, the most suitable materials for HCS are copper alloys and aluminum alloys. Therefore, the HCS does not need to control the thermal diffusivity but only needs to control the cooling capacity through the TEC controller.

With the continuous development of thermoelectric technology, the cooling power of a single thermoelectric cooling chip can reach several hundred watts and the size is very small, which is possible to design a TEC with high cooling power to cool high-power motorized spindle. Therefore, the TECS is better than traditional cooling system not only in terms of structural optimization but also in terms of cooling effect.

## 6. Conclusions

An optimization method for ThermoElectric-based Cooling System (TECS) has been proposed based on the conservation of energy. The cooling effect of TECS is verified and compared with water-cooling system through numerical simulation and thermal characteristics experiment. Based on the numerical simulation and experimental results, the following conclusions can be drawn.

1) The distribution of cooling capacity can be achieved by optimizing the contact area and position between the cooling channel and the spindle sleeve. The initial temperature field of spindle sleeve can be used to optimize the structure of cooling channel through calculating the over-cooled regions of the spindle sleeve.
2) Under the same conditions, the lower the temperature of the cooling channel, the more heat transfers from the internal heat sources to the cooling system, the better the cooling effect of the motorized spindle obtains, and there has a suitable temperature that makes the thermal elongation of spindle zero.
3) The stiffness of the motorized spindle is related to the structure and constraint mode and position, changing the restraint mode and position can greatly improve the stiffness of the system.

## Declarations

**Funding information** This paper is sponsored by the “Technology of on-line monitoring system for thermal characteristics of NC machine tools” (No. H2019304021); the “Project funded of Shanghai science committee- Precision technology and its application for five-axis machine tool based on the real-time compensation” (NO. J16022).

**Conflicts of interest/Competing interests** The authors declare that they have no conflict of interest.

**Availability of data and material** The data that supports the findings of this study is available from the corresponding author upon reasonable request.

**Code availability** Not applicable.

**Authors' contributions** The corresponding author contributed the central idea and wrote the initial draft of the paper. The remaining authors contributed to carrying out additional analyses and experiments and finalizing this paper.

**Ethics approval** The authors declare that the work is original and is not published elsewhere in any form or language.

**Consent to participate** The authors declare that they agree to participate.

**Consent for publication** The authors declare that they agree to publish.

## Reference

[1] Brecher C, Witt S. Static, dynamic and thermal behavior of machine tools with regard to HPC, CIRP High-Performance Cutting (2004) 227-242.
[2] Josef Mayr, Jerzy Jedrzejewski, Eckart Uhlmann, et al., Thermal issues in machine tools, CIRP Annals-Manufacturing Technology, 61(2) (2012) 771-791.

[3] Chao Jin, BoWu, Youmin Hu, Heat generation modeling of ball bearing based on internal load distribution, Tribology International, 45 (2012) 8-15.
[4] Jafar Takabi, M.M. Khonsari, Experimental testing and thermal analysis of ball bearings, Tribology International 60 (2013) 93-103.
[5] Vahid Norouzifard, Mohsen Hamedi, Experimental determination of the tool-chip thermal contact conductance in machining process, International Journal of Machine Tools & Manufacture, 84 (2014) 45-57.
[6] V. Gopal, M.J. Whiting, J.W. Chew, S. Mills, Thermal contact conductance and its dependence on load cycling, International Journal of Heat and Mass Transfer, 66 (2013) 444-450.
[7] J.H. Chow, Z.W. Zhong, W. Lin, L.P. Khoo, An investigation of thermal contact conductance using the lumped parameter method, International Journal of Thermal Sciences, 60 (2012) 114-121.
[8] K Kagata, K Kageyama, S Kinoshita, A Yoshida, Evaluation of thermal contact resistance between two solid surfaces using photoacoustic technique, International Journal of Thermophysics, 41 (2020) 131.
[9] Zhi Zhu, Li-Wen Zhang, Qin-Ke Wu, Sen-Dong Gu, An experimental investigation of thermal contact conductance of Hastelloy C-276 based on steady-state heat flux method, International Communications in Heat and Mass Transfer, 41 (2013) 63-67.
[10] Chang Ding, Rongshun Wang, Thermal contact conductance of stainless steel-GFRP interface under vacuum environment, Experimental Thermal and Fluid Science, 42 (2012) 1-5.
[11] Ishizaki T, Igami T, Nagano H, Measurement of local thermal contact resistance with a periodic heating method using microscale lock-in thermography, Review of Scientific Instruments, 91(6) (2020) 0640901.
[12] J.H. Chow, Z.W. Zhong, W. Lin, L.P. Khoo, The development of a simple semi-empirical method to obtain a predictive model of the convective heat loss of a solid surface of practical machine size by finite difference and experimentation, Applied Thermal Engineering, 75 (2015) 789-799.
[13] André Nozomu Sodoyama Barrios, João Batista Campus Silva, et al., Modeling heat transfer in die milling, Applied Thermal Engineering, 64 (2014) 108-116.
[14] H.T. Zhao, J.G. Yang and J.H. Shen, Simulation of thermal behavior of a CNC machine tool spindle, International Journal of Machine Tools & Manufacture 47 (2007) 1003-1010.
[15] Z.Z. Xu, X.J. Liu, H.K. Kim, J.H. Shin, S.K. Lyu, Thermal error forecast and performance evaluation for an air-cooling ball screw system, International Journal of Machine Tools & Manufacture, 51 (2011) 605-611.
[16] Y. Kang, X. Shi, J. Gao, F. Li, Modeling and analyzing multi-variable coupling thermal characteristics for motorized spindle, J Xi'an Jiaotong Univ, 50(8) (2016) 32-37.
[17] K. Fan, Research on the machine tool's temperature spectrum and its application in a gear form grinding machine, Int. J. Adv. Manuf. Technol. 90 (2017) 3841-3850.
[18] M.H. Xu, J. C. Cheng, S. Y. Zhang, Reconstruction theory of thermal conductivity depth profiles by the modulated photoreflectance technique, Journal of Applied Physics, 84(2) (1998)675-682.
[19] L.G. Page, J. Dirker, J.P. Meyer., Topology optimization for the conduction cooling of a heat-generating volume with orthotropic material. International Journal of Heat and Mass Transfer, 103 (2016) 1075-1083.
[20] K. Chen, S. Wang, M. Song, Optimization of heat source distribution for two-dimension heat conduction using bionic method, International Journal of Heat and Mass Transfer, 93 (2016) 108-117.
[21] Z Brodnianská, S Kotmíd, Intensification of convective heat transfer in new shaped wavy channel configurations, International Journal of Thermal Sciences, 162 (2021) 106794.
[22] Liu T, Gao WG, Tian YL, Zhang DW, Zhang YF, Chang WF, Power matching based dissipation strategy onto spindle heat generations, Applied Thermal Engineering, 113 (2017) 499-507.
[23] L Zhang, S Yu, Y Wu, K Zhang, Q Shi, D An, Parameter optimization of a motorized spindle lubrication system using biogeography-based optimization, Advances in Mechanical Engineering, 11(1) (2019) 1-11.
[24] Yanru Zhang, Longyun Zheng, Wenzhe Qi, Kai Guo, Hui Liu, Chunjiang Liu, Optimal design of a multi-branch conducting path for area-to-point heat conduction using multi-objective optimization, Applied Thermal Engineering, 125 (2017) 1354-1367.
[25] Hao Zhou, Kaiguo Fan, Rui Gao, Fast heat conduction-based thermal error control technique for spindle system of machine tools, The International Journal of Advanced Manufacturing Technology, 107 (2020) 653–666.
[26] Zhi Zhu, Li-Wen Zhang, Qin-Ke Wu, Sen-Dong Gu, An experimental investigation of thermal contact conductance of Hastelloy C-276 based on steady-state heat flux method, International Communications in Heat and Mass Transfer, 41 (2013) 63-67.
[27] Chang Ding, Rongshun Wang, Thermal contact conductance of stainless steel-GFRP interface under vacuum environment, Experimental Thermal and Fluid Science, 42 (2012) 1-5.
[28] V. Gopal, M.J. Whiting, J.W. Chew, S. Mills, Thermal contact conductance and its dependence on load cycling, International Journal of Heat and Mass Transfer, 66 (2013) 444-450.
[29] J.H. Chow, Z.W. Zhong, W. Lin, L.P. Khoo, An investigation of thermal contact conductance using the lumped parameter method, International Journal of Thermal Sciences, 60 (2012) 114-121.
[30] ISO 230-3:2020, Test code for machine tools-Part 3: Determination of thermal effects, 2020.
[31] L. Wu, Q. Tan, Thermal characteristic analysis and experimental study of a spindle-bearing system, entropy, 18(7) (2016) 271.